Characteristics of Selective Chemical Vapor Deposition of Tungsten on Aluminum with a Vapor Phase Precleaning Technology

Kow-Ming Chang, Ta-Hsun Yeh, Shih-Wei Wang, and Chii-Horng Li

Department of Electronics Engineering and Institute of Electronics, National Chiao Tung University and National Nano Device Laboratory, Hsinchu, Taiwan

ABSTRACT

A simple and efficient precleaning of an aluminum surface with hydrochloric acid vapor prior to selective chemical vapor deposition of tungsten was investigated. The vapor phase precleaning was shown to remove the aluminum native oxide as well as reduce the aluminum fluorides formed at the W/Al interface during initial reaction of WF_6 with the aluminum underlayer. It was found that the precleaning process is spontaneous and the removal rate of aluminum is related to the concentration of reactants used. After precleaning, the aluminum surface was free of oxide and covered with a large amount of Cl species that were examined by x-ray photoelectron spectroscopy. These Cl species occupy active sites on the wafer surface and prevent further adsorption of WF_6 on the aluminum during the initial stage in selective deposition of tungsten. Therefore, the probability of reaction between WF_6 and the underlying aluminum is greatly suppressed. By using a hydrochloric acid vapor to pretreat the aluminum trench and via hole patterned substrates, a smooth and dense tungsten film and low selectivity loss (<50 pcs/cm^2) were obtained. A low concentration of aluminum fluorides accumulated at the W/Al interface that were involved in low via resistance was also observed.

Introduction

Chemical vapor deposition of tungsten (CVD-W) has been proposed to be an important metallization technique in ultralarge-scale integrated circuit (ULSI) applications.[1-6] By controlling reaction parameters, the process can be made to deposit tungsten selectively on silicon or on other metals but not on SiO_2 or other insulators.[2,7-9] In this work, a selective CVD-W film directly deposited on aluminum for via fills by using WF_6/SiH_4 reduction was investigated. Previous workers[4,10,11] have reported that the nucleation of CVD-W on aluminum can be suppressed or blocked entirely due to the existence of a thin Al native oxide. In general, *in situ* plasma sputtering[11-13] and reactive ion etching (RIE) have been used extensively to remove the native metal oxide prior to conducting the CVD-W. During the plasma precleaning, however, the outsputtered aluminum oxide and aluminum can be redeposited on the sidewalls of the trench and via hole and on the surface of the dielectric layer, where tungsten nucleation is induced, resulting in creep-up and selectivity loss during tungsten deposition. In addition, hot concentrated hydrochloric acid solution has also been proven by Ng *et al.*[14] to provide an effective precleaning. Nevertheless, for devices in the deep submicron regime where contacts/vias have high aspect ratios, wet precleaning exhibits severe problems such as wetting, surface tension, and bubble formation.

Typically, the initial reaction pathway of CVD-W on aluminum for via fills can be summarized as follows

$$WF_6 + 2Al \rightarrow W + AlF_3 \qquad \Delta G(500\ K) = -1163\ kJ/mol \qquad [1]$$

$$2AlF_3 + Al \rightarrow 3AlF_2\uparrow \qquad (>350°C) \qquad [2]$$

The Al reduction of WF_6 takes place preferentially to SiH_4 and H_2 reduction of WF_6 due to the more negative free energy of Al reduction compared to SiH_4 and H_2 reduction[15]

$$WF_6 + 3H_2 \rightarrow W + 6HF \qquad \Delta G(500\ K) = -113\ kJ/mol \qquad [3]$$

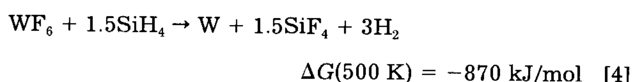

$$WF_6 + 1.5SiH_4 \rightarrow W + 1.5SiF_4 + 3H_2 \qquad \Delta G(500\ K) = -870\ kJ/mol \qquad [4]$$

Moreover, nonvolatile aluminum trifluoride (AlF_3) formed on the aluminum surface during the initial reaction of WF_6 with aluminum can dramatically degrade the CVD-W/Al contact properties. A general solution could be application of additional glue layers (*e.g.*, TiN) on Al[16,17] or higher deposition temperature[18] (formation of volatile AlF_2 from AlF_3). In this study, we develop a simple but efficient precleaning technology to remove the Al native oxide and to suppress the AlF_3 accumulated at the W/Al interface by using hydrochloric acid vapor precleaning. The Al surface after precleaning is free of oxide and covered with a chlorine-terminated layer. Furthermore, this vapor phase precleaning is able to eliminate the wetting problems of vias with high aspect ratio in wet precleaning as well as to solve the issues of creep-up and selectivity loss that occur with plasma sputtering and RIE precleanings.

Experimental

Aluminum alloy (Al-1%Si-0.5%Cu) was sputter-deposited on thermally oxidized silicon wafers to a thickness of 500 nm. A 50 nm thick TiN was also sputtered over the aluminum layer as the antireflection layer (ARL). The ARL assists in forming well-resolved, fine line resist images that are free of notching and necking.[19] The sample with a TiN/AlSiCu bilayer was patterned by Cl_2/BCl_3-based RIE. After removing the photoresist on the TiN/AlSiCu bilayer with a solution of N-methyl pyrrolidone and 2-ethanol, it was covered with dielectric layers of 200 nm plasma-enhanced chemical vapor deposited (PECVD) oxide, 300 nm spin-on-glass (SOG), and 500 nm PECVD oxide. Through sequential photolithography processes and patterning with fluorocarbon-based RIE chemistry, a set of via holes and trenches with sizes ranging from 0.5 to 5 μm can be obtained. The 50 nm TiN layer which would have increased the via resistance was removed during RIE of the via hole. Meanwhile, unpatterned CVD-W/Al samples were fabricated for physical characterization.

Prior to selective CVD-W processing, the wafers were treated with various precleans. The (a) group of wafers was treated by HCl vapor phase precleaning. This process involved a 2:1 mixture of 35%HCl:H_2O in a sealed container, as shown in Fig. 1. The hot plate was kept at 50°C to vaporize the solution. After reaching steady state, we opened the valve to achieve 30 to 120 s of vapor exposure on wafer. The wafer was then loaded into the CVD-W system as soon as possible. Another group of wafers (b) was dipped in 50°C aqueous HCl solution (35%HCl:H_2O = 1:1) for 20 s, followed by a 5 min DI water rinse and spin dry. The third group of wafers (c) was treated with *in situ* SF_6/BCl_3 plasma etching in the CVD system. The redeposition plasma etching was conducted with a radio frequency (RF) power of 100 W, $SF_6/BCl_3/N_2$ flow rates of 10/10/100 sccm, chamber pressure 20 mTorr, and 30 s time.

Downloaded on 2014-04-28 to IP 140.113.38.11 address. Redistribution subject to ECS terms of use (see ecsdl.org/site/terms_use) unless CC License in place (see abstract).

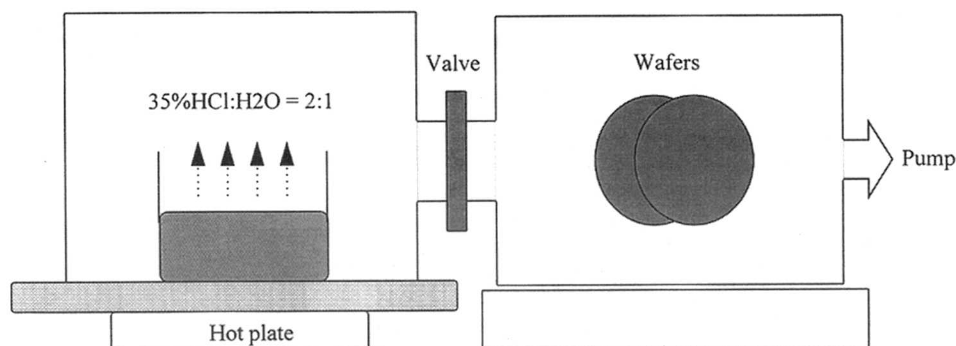

Fig. 1. The diagram of experimental configuration for vapor phase precleaning.

The (d) group of wafers was control samples without precleaning before tungsten deposition. Finally, all wafers were loaded into the load-locked coldwall CVD-W system to deposit tungsten film. The base pressure of the CVD-W chamber (ULVAC ERA-1000 system) was 10^{-6} Torr, and the laminarized gas flow system was designed to greatly reduce reactor wall contamination. Typical deposition parameters for the selective CVD-W in this work were 20 mTorr in pressure and a substrate temperature of 350°C (substrate heating with infrared lamp). The flow rates of WF_6 and SiH_4 were 20 and 12.5 sccm, respectively, without any carrier gas.

For analyses, we employed scanning electron microscopy (SEM), secondary ion mass spectroscopy (SIMS), x-ray photoelectron spectroscopy (XPS), and x-ray diffractometry (XRD) as tools to examine the CVD-W film morphology, the impurities in the CVD-W/Al bilayer, the bonding structures on the aluminum surface after HCl vapor precleaning, and the CVD-W crystalline phase, respectively. Concurrently, via resistance was measured using a four-terminal Kelvin structure prepared by the conventional ULSI process where the via holes were 0.6 μm deep and 1.2 to 5 μm diam.

Results and Discussion

The first paper describing vapor phase etching was written by Holmes and Snell[20] in 1966. They employed the HF vapor to remove silicon oxide. Many subsequent researchers[21-23] also investigated a process based on vapor phase of a HF/H_2O mixture for etching SiO_2. The main advantages of vapor cleaning are that it reduces contaminant redeposition and improves process uniformity.[24] Similarly, we apply the vapor phase of a HCl/H_2O mixture to remove alumimum surface oxide. This vapor phase cleaning is a spontaneous process because the diatomic bond strength of H-Cl (431 kJ/mol) is smaller than that of Al-Cl (506 kJ/mol). Figure 2 reveals the removal rate of aluminum exposed under the vapor of HCl solution with various concentrations. The removal rates of aluminum were calculated from the quotient of 10 min etched aluminum thickness that was examined by SEM and 10 min of exposure time. It is noted that there was a critical volume ratio of HCl to H_2O to achieve an efficient cleaning and the etching behavior is quenched while the volume ratio is higher than 3:1 (*i.e.,* 5:1 and 10:1 conditions in Fig. 2). This result is hypothetically similar to the mechanism of gas phase etching of silicon oxide with HF gas.[25,26] An HCl molecule does not ionize in a completely moisture-free gas phase environment. However, the etching reaction can be considered to be triggered by HCl molecule ionization at the aluminum surface due to remaining adsorbed moisture molecules. Thus, the reaction is proposed as follows

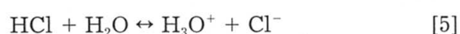

$$HCl + H_2O \leftrightarrow H_3O^+ + Cl^- \quad [5]$$

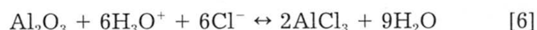

$$Al_2O_3 + 6H_3O^+ + 6Cl^- \leftrightarrow 2AlCl_3 + 9H_2O \quad [6]$$

The presence of H_2O on aluminum native oxide surfaces initiates the ionization of the HCl molecule, and the aluminum oxide reacts with the generated Cl^- ion, which leads to a generation of more H_2O. The generated H_2O enhances the ionization reaction of the HCl molecules, resulting in an increase of Cl^- ions. This positive feedback mechanism causes the rapid rise in the aluminum removal rate at the critical HCl volume ratio. As a result, in the absence of moisture to trigger HCl ionization, the cleaning behavior will be restrained under the condition of high volume ratio of HCl to H_2O. Moreover, the lower volume ratio conditions can decrease the HCl molecule concentration in a gas-phase environment. Lower removal rates are thus obtained.

Figure 3a-c shows the XPS spectra of Al (2p), O (1s), and Cl (2p) for aluminum with different precleanings, respectively. It is found that the sample treated with 60 s of vapor phase precleaning [*i.e.,* wafer (a)-60 s] exhibits the highest intensity of Cl as well as the lowest intensities of O and Al_2O_3 peaks. The result indicates that the HCl vapor-exposed Al surface was free of oxide and covered with a large amount of Cl species. In addition, the trivial oxygen on wafer (a)-60 s is speculated to be from the reoxidation process during wafer transport under atmospheric ambient before loading into the XPS analyzer. Meanwhile, the (a)-30 s sample gave similar results except it displayed insufficient cleaning (*i.e.,* higher intensity of oxygen signal than that of wafer (a)-60 s). For the (b) group, the quantities of Al-OH bonds were formed on the aluminum surface through the hydrolysis of H_2O during the DI water rinsing step. These Al-OH bonds then condense into AlO_x, and thus a thin oxide rapidly regrows on the aluminum. It causes the high O (1s) and low Cl (2p) intensities on the

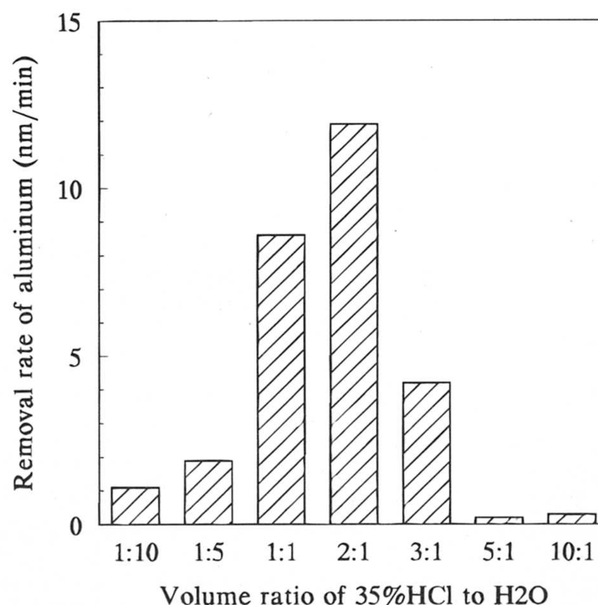

Fig. 2. The removal rates of aluminum exposed under the vapor of HCl solution with various concentrations.

Downloaded on 2014-04-28 to IP 140.113.38.11 address. Redistribution subject to ECS terms of use (see ecsdl.org/site/terms_use) unless CC License in place (see abstract).

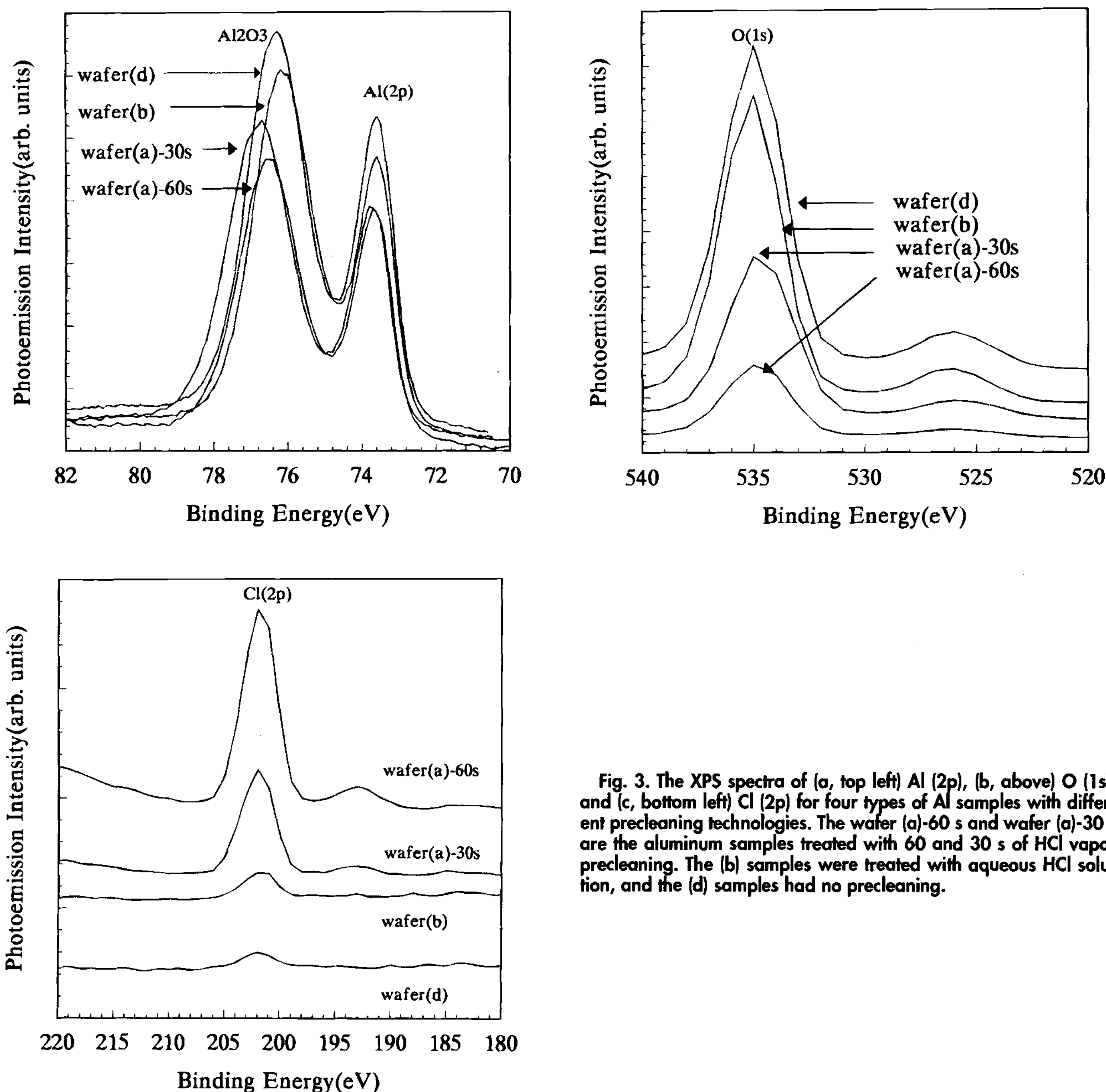

Fig. 3. The XPS spectra of (a, top left) Al (2p), (b, above) O (1s), and (c, bottom left) Cl (2p) for four types of Al samples with different precleaning technologies. The wafer (a)-60 s and wafer (a)-30 s are the aluminum samples treated with 60 and 30 s of HCl vapor precleaning. The (b) samples were treated with aqueous HCl solution, and the (d) samples had no precleaning.

aluminum surface (as shown in Fig. 3b and c) even after precleaning with aqueous HCl solution.

The selective CVD-W films on submicron trenches and via holes down to aluminum with various precleanings were also investigated, and the results are summarized in Table I. The measured deposition rates are the thickness of tungsten films directly deposited on the unpatterned aluminum substrate with 60 s of deposition time, however, not the thickness within trenches and via holes. Figure 4 demonstrates the grain structures of CVD-W films deposited on aluminum with different precleanings. The samples treated with vapor phase precleaning (Fig. 4a and b) have higher deposition rates, denser structures, lower resistivity (≅13 μΩ cm), and smoother morphologies than

Table I. Selective CVD-W on submicron trenches and via holes with various precleanings.

	Wafer group (a) HCl vapor precleaning			Wafer group (b) Aqueous HCl solution dip	Wafer group (c) *In situ* SF_6/BCl_3 plasma precleaning	Wafer group (d) Without any precleaning
	30 s	60 s	120 s			
Grain structure and film morphology	Fig. 4b	Fig. 4a	Fig. 5	Fig. 4c		Fig. 4d
Deposition rate (nm/min)	393	450		356		243
Via hole fills		Fig. 6a Fig. 7a		Fig. 6b	Fig. 7b	No deposition
Trench fills		Fig. 7a			Fig. 7b	No deposition
Selectivity loss		<50 pcs/cm^2 Fig. 8a		>200 pcs/cm^2 Fig. 8b	High selectivity loss Fig. 8c	Blanket deposition (No deposition in via hole)
SIMS depth profiles of CVD-W/Al structure		Fig. 9a			Fig. 9b	
X-ray diffraction patterns				Fig. 10		

Downloaded on 2014-04-28 to IP 140.113.38.11 address. Redistribution subject to ECS terms of use (see ecsdl.org/site/terms_use) unless CC License in place (see abstract).

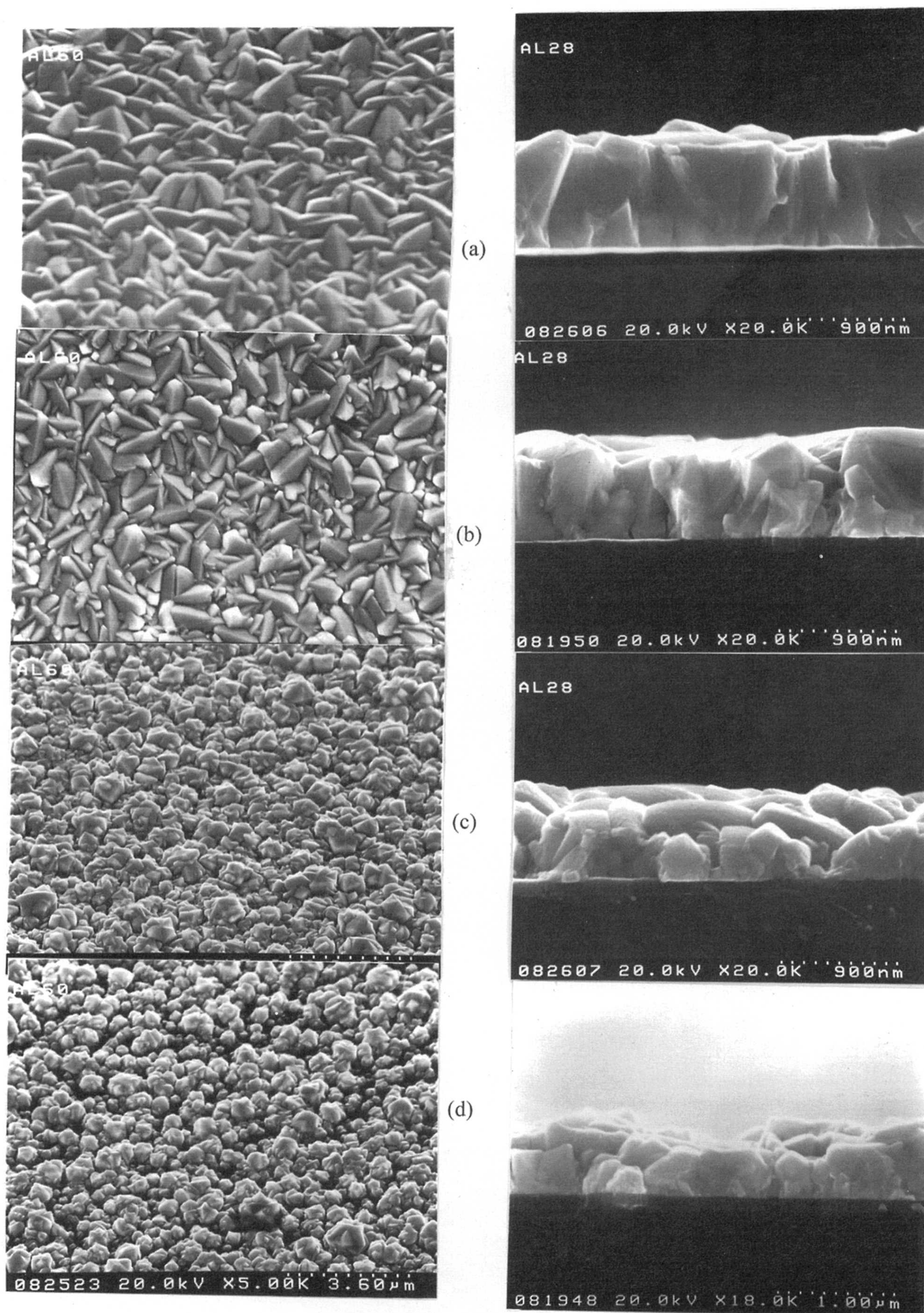

Fig. 4. The SEM micrographs of CVD-W films on aluminum with different precleanings. Figures (a) and (b) show the aluminum samples treated with 60 and 30 s of HCl vapor precleaning, respectively, (c) shows the (b) wafers, and (d) the (d) wafers. The selective CVD-W deposition parameters are 20 mTorr pressure and 350°C substrate temperature. The flow rates of WF_6 and SiH_4 are 20 and 12.5 sccm, and the deposition time is 120 s.

Downloaded on 2014-04-28 to IP 140.113.38.11 address. Redistribution subject to ECS terms of use (see ecsdl.org/site/terms_use) unless CC License in place (see abstract).

those of other samples. On the other hand, the groups of wafers (b) and (d) represent similar characteristics, as exhibited in Fig. 4c and d. The as-deposited CVD-W films gave porous, equiaxed, and island-like surface morphology, which was due to the unremoved aluminum surface oxide that inhibited the nucleation of W. Nevertheless, an overlong vapor phase precleaning would induce the coagulation of moisture in vapor on the wafer surface. The Al-Cl species on aluminum were hydrolyzed to Al-OH bonds by the excess moisture. While these Al-OH species condensed into AlO_x, the aluminum surface was reoxidized again. Figure 5 reveals the SEM micrograph for the CVD-W deposited on Al with 120 s of vapor phase precleaning. Obviously, the right side of picture has the elongate and dense W grains. On the contrary, the left side of picture where the moisture condenses on the wafer, shows the equiaxed island-like W grains and is even without deposition. This phenomenon was caused by a thin oxide regrown on the aluminum after an overlong vapor phase precleaning.

When the devices are scaled down for ULSI circuit applications, many problems take place in wet cleaning technology. The via holes with small size and high aspect ratios will encounter the issues of cleaning such as wetting, surface tension, and bubble formation. As shown in Fig. 6, the (a) group of wafers shows excellent deposition and fine grain structures for 0.6 μm size via fills as opposed to the (b) wafers. The belly-shaped via is caused by the different etching rates between SOG and PECVD oxides during the via etching. The faulty deposition of tungsten in the (b) group is because the precleaning was blocked by wetting, and surface tension issues and the removal of aluminum native oxide was then uncompleted.

Except for wet precleaning, other precleaning techniques using plasma sputtering[12-14] or reactive ion etching have been extensively studied. Nevertheless, the etching products (aluminum-containing complexes) formed in the cleaning step could be redeposited on the sidewalls of the trenches and via holes and on the surface of the PECVD oxide. When the reactants (*i.e.*, WF_6 and SiH_4) of CVD-W were introduced, the WF_6 could react with these products to form W. Simultaneously, the SiH_4 adsorbed on etching products would dissociate into Si atoms and then react with WF_6 to nucleate W. Both reactions result in the creep-up and selectivity loss during selective deposition of tungsten. Figure 7 reveals the SEM micrographs of selective CVD-W for trench and via fills. It is noted that the (c) wafers show an obvious creep-up, failed via fills, and selectivity loss. By contrast, the (a) group possessed superior deposition and selectivity. Figure 8 demonstrates the selectivity of selective CVD-W for via fills with various precleanings. The selectivity loss defines the number of tungsten particles which deposit on the PECVD oxide per cm^2, and we used a dark field optical microscope to count the particles. For the sake of accuracy, we averaged the values of five positions (right, left, center, top, and bottom) on the whole wafer. Every position is 1 cm^2 in area. The statistical values are listed in Table I. The (a) group (Fig. 8a) shows the completely selective deposition of tungsten, while the (b) group reveals imperfect deposition. In addition, the selectivity of group (b) is inferior to that of group (a). The mechanism of selectivity loss of wafer (b) is guessed due to the redeposition of the contaminants in the aqueous HCl solutoin and DI water during precleaning. These contaminants could act as the nucleation sites for W deposition in the sequential CVD-W process. For the case of wafer group (c) with *in situ* plasma precleaning, a grave selectivity loss was observed in Fig. 8c. (The detailed cause was clarified in the above-mentioned discussion.) At the same time, the (d) group (*i.e.*, the sample without any precleaning) showed a blanket deposition of tungsten on the PECVD oxide and no deposition of W inside the via holes.

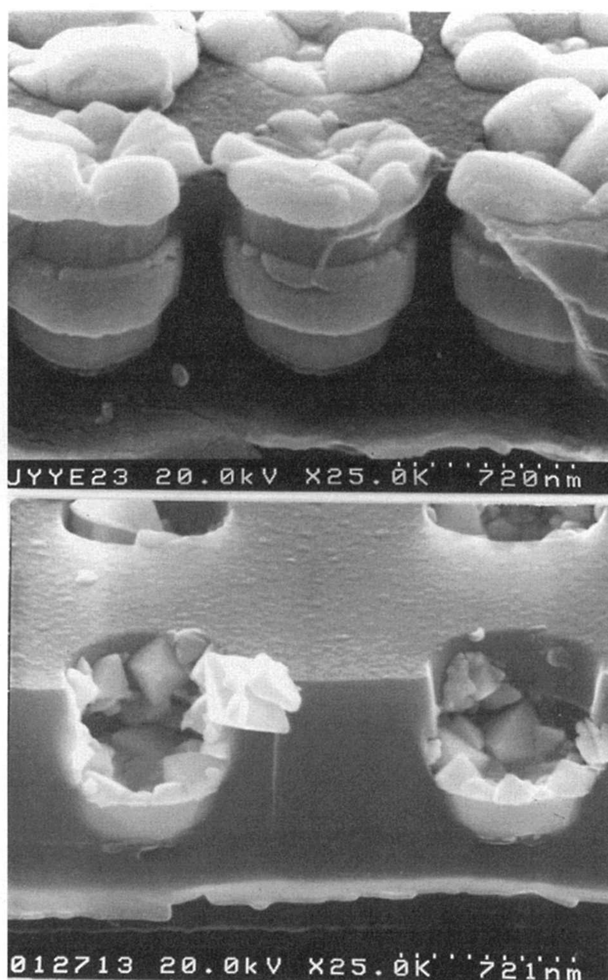

Fig. 6. The SEM micrographs for via fills: (a, top) the (a) group of wafers and (b, bottom) the (b) group. Deposition parameters are the same as Fig. 4.

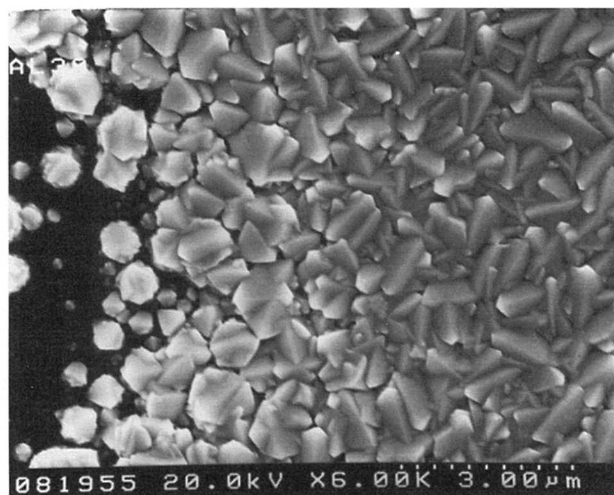

Fig. 5. SEM micrograph of CVD-W film on Al for the sample precleaned with 120 s of HCl vapor. The deposition parameters are the same as Fig. 4.

Furthermore, one inherent problem with the CVD-W process for via filling application is the aluminum trifluorides formed by the initial aluminum reduction with WF_6 that act as an insulating layer at the CVD-W/Al interface and then greatly degrade the contact properties between CVD-W and aluminum. Previous workers[16,17] have used an additional glue layer (*e.g.*, TiN) on aluminum as a barrier layer to halt the direct reaction between Al and WF_6. In

Downloaded on 2014-04-28 to IP 140.113.38.11 address. Redistribution subject to ECS terms of use (see ecsdl.org/site/terms_use) unless CC License in place (see abstract).

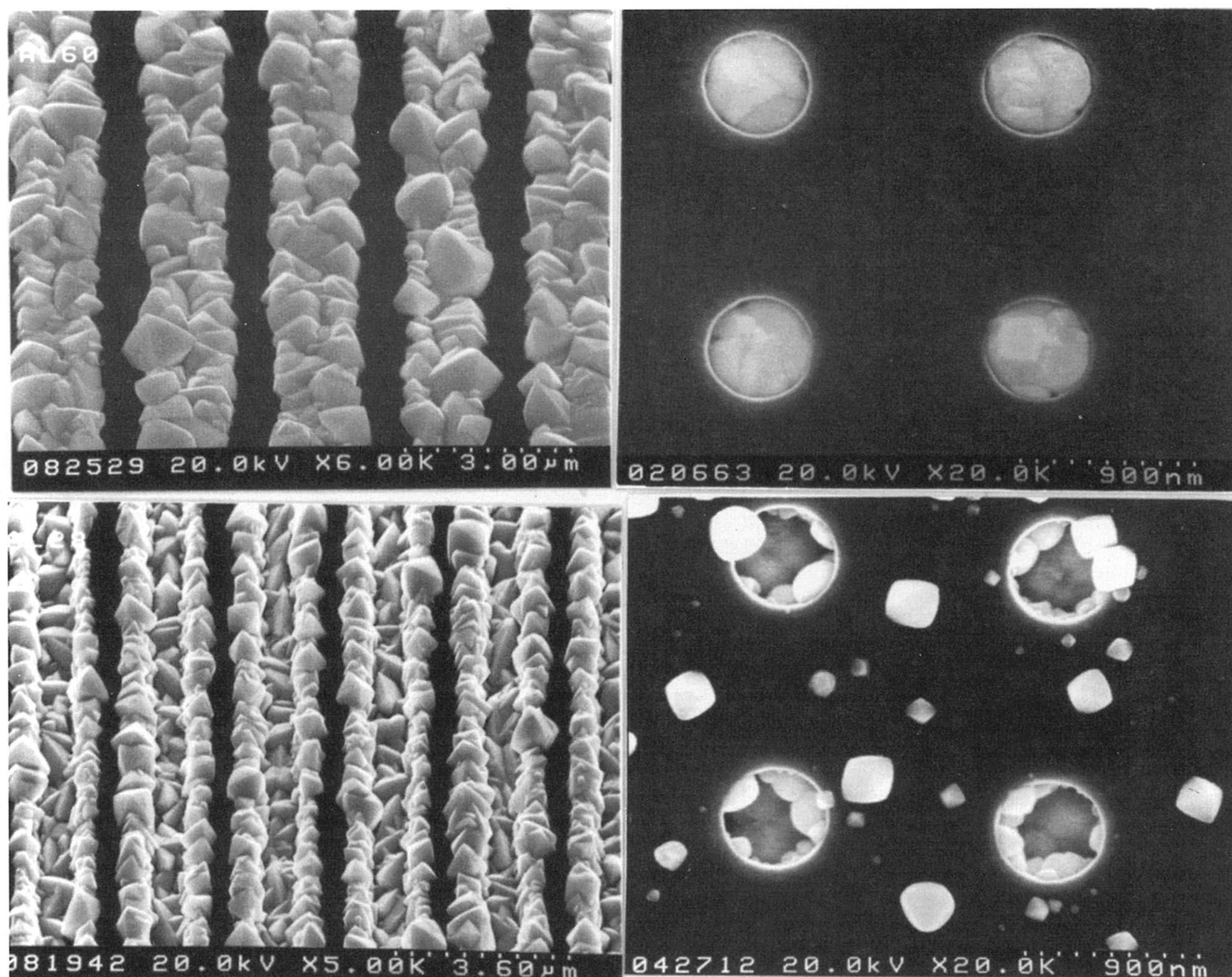

Fig. 7. SEM micrographs for trench and via fills: (a, top row) the (a) group of wafers and (b, bottom row) for the (c) group. The deposition parameters are 20 mTorr pressure and 350°C substrate temperature. The flow rates of WF_6 and SiH_4 are 20 and 12.5 sccm, respectively, and the deposition time is 100 s.

addition, elevating the deposition temperature[18] has also proven to enhance the desorption of AlF_3 from the aluminum surface through formation of volatile AlF_2. However, the additional glue layer complicates the process and increases the cost, and the high deposition temperature is not compatible with the presence of the underlying aluminum layer.

In this study, we have also found that the vapor phase precleaning could reduce the aluminum fluorides pileup at the CVD-W/Al interface. Figure 9a and b illustrates the SIMS depth profiles of CVD-W/Al structures with different precleanings prior to tungsten deposition. The F concentration of the (a) group is one order lower than that of the (c) group. At the same time, the impurities of Si and O in the tungsten films of (a) are also lower than those of (c). It is conjectured that the Cl species cover the aluminum after HCl vapor precleaning and occupy the surface active sites to prevent further adsorption of WF_6 on Al. The succeeding SiH_4 reduction could take place immediately to form a W seed layer, because the negative free energy of SiH_4 reduction was close to that of Al reduction. Accordingly, the probability of a direct reaction between the WF_6 and the underlying Al was suppressed. However, the HCl vapor phase precleaning cannot completely eliminate the fluoride pileup at the W/Al interface. Some Cl species were evaporated during the heating step in the deposition process and were replaced by F species when WF_6 was dissociated on the aluminum surface. A slightly high concentration of F was thus observed at the CVD-W/Al interface, as indicated in Fig. 9a.

We have examined the x-ray diffraction patterns for the CVD-W (500 nm) films deposited on the unpatterned aluminum treated with various precleanings. As shown in Fig. 10, the (a) group possesses the strongest peak (110) α-W peak without β-phase tungsten detected. However, the wafers in group (b) and (c) reveal obvious peaks that correspond to the metastable β-W phase. It is known that the β-W lattice is stabilized by impurities like fluorine,[29] oxygen,[3] and silicon.[30] These impurities are either from the adequate precleaning procedure prior to CVD-W deposition or are affected by the growth conditions. In our case of keeping the same deposition parameters through whole experiments, the precleaning should be the dominant factor that determines the crystalline phase of as-deposited tungsten films. Therefore, the β-W peaks in groups (b) and (c) were conceivably induced by the discrepancy of precleaning effectiveness.

Finally, the electrical characteristics of via resistance were measured using a four-terminal Kelvin structure of an AlSiCu/W/AlSiCu device. The top view and cross-sectional diagrams of a four-terminal D-type Kelvin test structure[27,28] with W-plugs are shown in Fig. 11a. For via resistance measurement, current I_{13} was forced through pads 1 and 3, and the via resistance R was determined by sensing the voltage drop V_{24} between pads 2 and 4 through the relation $R = V_{24}/I_{13}$. Figure 11b illustrates the meas-

Downloaded on 2014-04-28 to IP 140.113.38.11 address. Redistribution subject to ECS terms of use (see ecsdl.org/site/terms_use) unless CC License in place (see abstract).

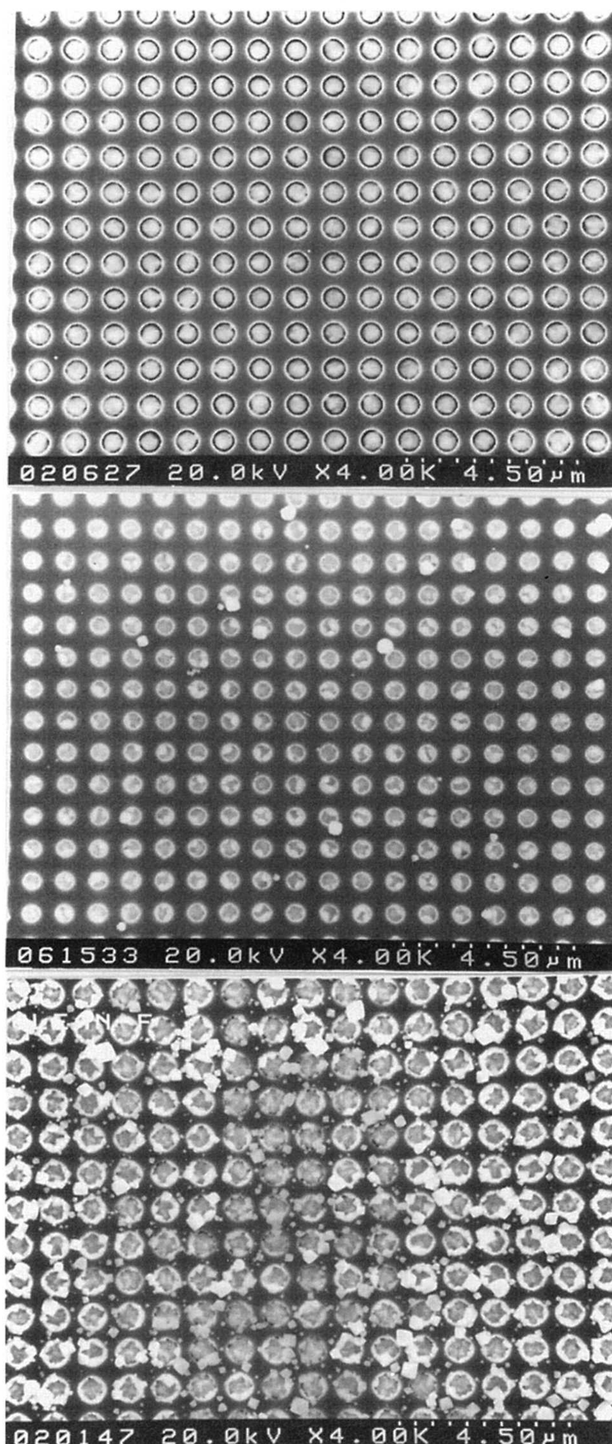

Fig. 8. The selectivity loss of selective CVD-W for via fills with various precleanings: (a, top) for the (a) group, (b, middle) for the (b) group, and (c, bottom) for the (c) group. Deposition parameters are the same as Fig. 7.

ured via resistance *vs.* via size for samples with different precleanings prior to CVD-W. We have known that the via resistance of the W-plug device was affected by the cleanness of the CVD-W/Al interface as well as by the resistivity of the W-plug itself. Clearly, the (a) wafers exhibit lower via resistance than the other samples. This is attributed to the reoxidation of the aluminum surface of the group (b) wafers during the DI water rinse step of precleaning. Similarly, the (c) wafers suffer a larger amount of AlF_3 formed at the CVD-W/Al interface, resulting in high via resistance.

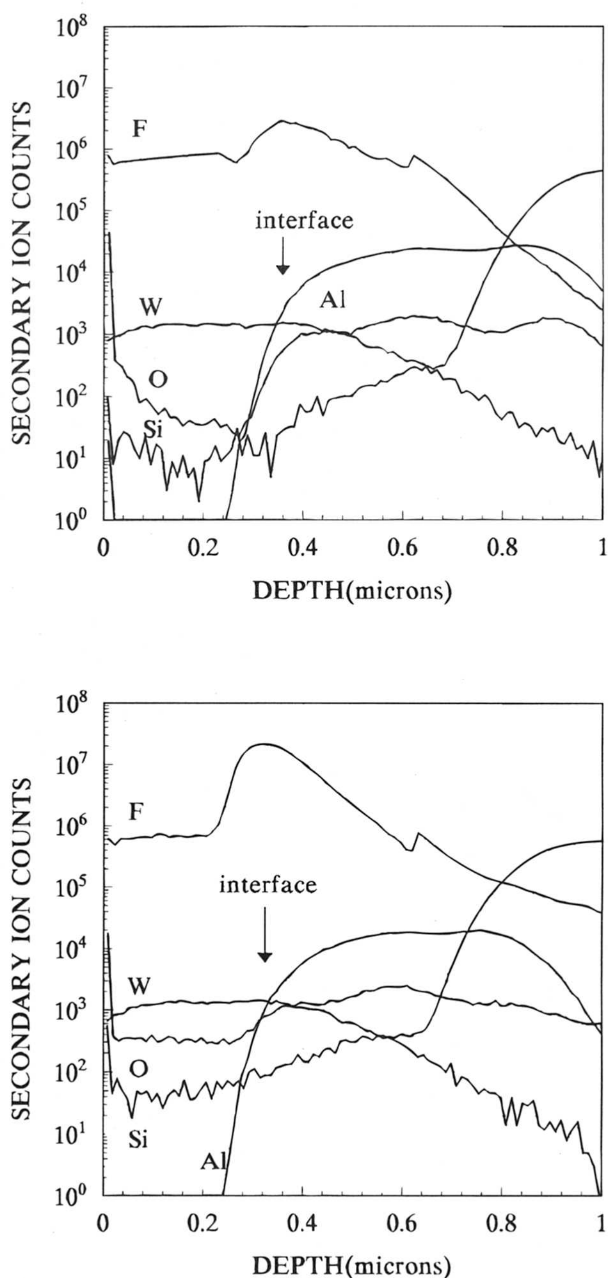

Fig. 9. The SIMS depth profiles of CVD-W/Al structures with different precleaning techniques prior to tungsten deposition: (a, top) the (a) group, and (b, bottom) the (c) group of wafers.

Summary

A simple and efficient precleaning using hydrochloric acid vapor prior to selective deposition of tungsten on Al has been shown to remove Al native oxide and to suppress the aluminum fluorides formed at CVD-W/Al interfaces. A large amount of Cl species were detected on the aluminum surface after HCl vapor precleaning, and the removal rate of aluminum was related to the concentration of reactants used. Moreover, vapor phase precleaning can solve the problems of wetting and bubble formation that occur during wet precleaning for filling vias with small size and high aspect ratio. It can also eliminate creep-up and selectivity loss induced by precleaning using *in situ* plasma sputtering or RIE. Our results show a high deposition rate and dense and smooth CVD-W films with low resistivity and low concentration of F formed at the CVD-W/Al interface, resulting in low via resistance.

Downloaded on 2014-04-28 to IP 140.113.38.11 address. Redistribution subject to ECS terms of use (see ecsdl.org/site/terms_use) unless CC License in place (see abstract).

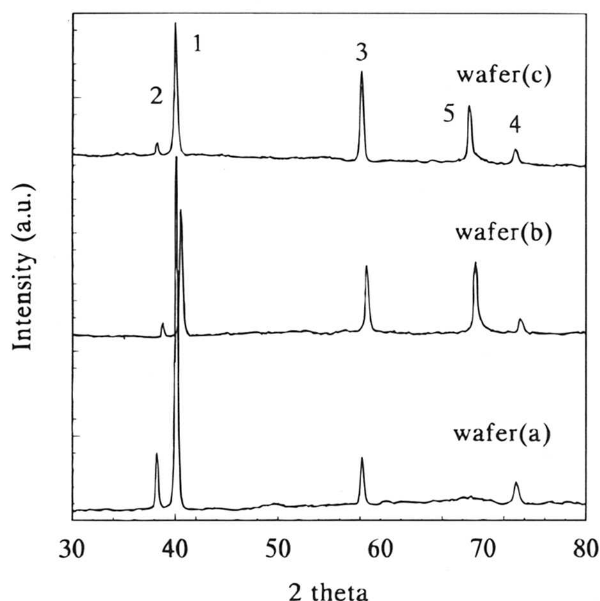

Fig. 10. The XRD patterns of selective CVD-W (500 nm) films deposited on the unpatterned aluminum treated with various precleanings: (1) α-W(110), (2) Al(111), (3) α-W(200), (4) α-W(211), and (5) β-W(321).

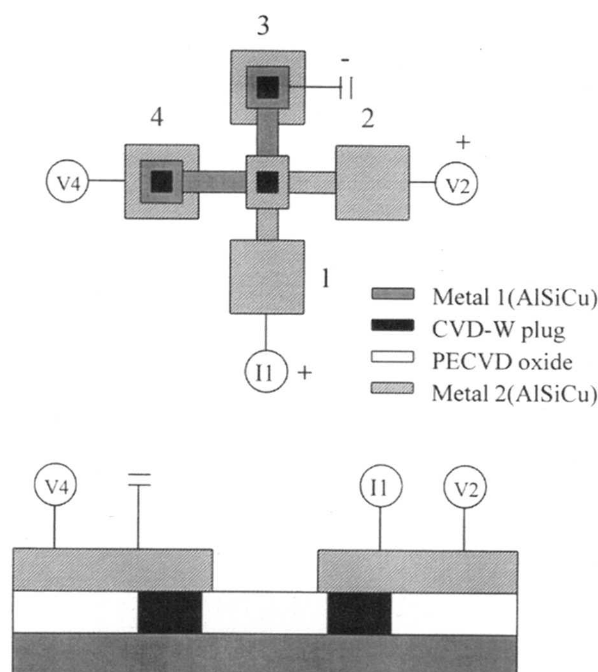

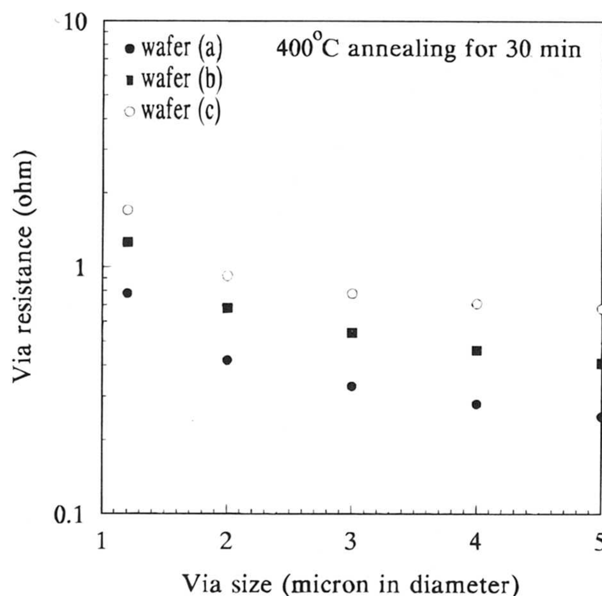

Fig. 11. (a, top) Top view and cross-sectional diagrams of a D-type four-terminal Kelvin test structure for measuring via resistance of the AlSiCu/W/AlSiCu device. (b, bottom) Via resistance *vs.* via size for three samples with different precleanings.

Acknowledgments

This work is supported by National Science Council, Taiwan, under Grant No. NBC 85-2215-E-009-061.

Manuscript submitted Jan. 16, 1996; revised manuscript received Oct. 14, 1996.

National Chiao Tung University assisted in meeting the publication costs of this article.

REFERENCES

1. J. E. J. Schmitz, *Chemical Vapor Deposition of Tungsten and Tungsten Silicides for VLSI/ULSI Application,* Chap. 1, Noyes Publications, Park Ridge, NJ (1991).
2. E. K. Broadbent and C. L. Ramiller, *This Journal,* **131,** 1427 (1984).
3. H. H. Busta and C. H. Tang, *ibid.,* **133,** 1195 (1986).
4. M. Wong, N. Kobayashi, R. Browning, D. Paine, and K. C. Sarawat, *ibid.,* **134,** 2339 (1987).
5. M. L. Yu, K. Y. Ahn, and R. V. Joshi, *J. Appl. Phys.,* **67,** 1055 (1990).
6. M. L. Yu and B. N. Eldrige, *J. Vac. Sci. Technol.,* **A7,** 626 (1989).
7. T. Tsutsumi, H. Kotani, J. Komori, and S. Nagao, *IEEE Trans. Electron. Devices,* **ED-37,** 569 (1990).
8. J. M. DeBlasi, D. K. Sadana, and M. H. Norcott, *Mater. Res. Symp. Proc.,* **71,** 303 (1986).
9. E. K. Broadbent and W. T. Stacy, *Solid-State Technol.,* **28,** 51 (1985).
10. E. K. Broadbent, *J. Vac. Sci. Technol.,* **B5,** 1661 (1987).
11. V. V. S. Rana, J. A. Taylor, L. H. Holschwandner, and N. S. Tsai, in *Tungsten and Other Refractory Metals for VLSI Applications III,* Victor A. Wells, Editor, p. 187, MRS, Philadelphia, PA (1987).
12. R. C. Ellwanger, J. E. J. Schmitz, and A. J. M. Van Dijk, *ibid.,* p. 399.
13. E. Nishitani and S. Tsuzuku, in *Tungsten and Other Advanced Metals for VLSI/ULSI Applications V,* S. S. Wong and S. Furukawa, Editors, p. 61, MRS, Philadelphia, PA (1989).
14. S. L. Ng, S. J. Rosner, D. R. Bradbury, T. I. Kamins, and S. S. Laderman, in *Tungsten and Other Refractory Metals for VLSI Applications II,* E. K. Broadbent, Editor, p. 93, MRS, Philadelphia, PA (1986).
15. D. R. Bradbury, J. E. Turner, K. Nauka, and K. Y. Chiu, *IEDM Proc.,* 273 (1991).
16. M. L. Yu, K. Y. Ahn, and R. V. Joshi, in *Tungsten and Other Refractory Metals for VLSI Applications II,* E. K. Broadbent, Editor, p. 93, MRS, Philadelphia, PA (1986).
17. M. L. Yu, K. Y. Ahn, and R. V. Joshi, *IBM J. Res. Develop.,* **34,** 875 (1990).
18. D. Alugbin, D. Favreau, D. Kostelnick, K. Olasupo, and J. Shimer, in *Tungsten and Other Refractory Metals for VLSI Applications II,* E. K. Broadbent, Editor, p. 93, MRS, Philadelphia, PA (1986).
19. P. E. Riely, S. S. Peng, and L. Fang, *Solid-State Technol.,* **36,** 47 (1993).
20. P. J. Holmes and J. E. Snell, *Microelectron. Reliab.,* **5,** 377 (1966).
21. R. E. Novak, *Solid-State Technol.,* **31,** 41 (March 1988).
22. B. E. Deal, M. A. McNerlly, D. B. Kao, and J. M. deLarios, *ibid.,* **33,** 73 (July 1990).
23. C. R. Cleavelin and G. T. Duranko, *Semicond. Int.,* 94 (Nov. 1987).
24. B. E. Deal and C. R. Helms, *Handbook of Semicon-*

Downloaded on 2014-04-28 to IP 140.113.38.11 address. Redistribution subject to ECS terms of use (see ecsdl.org/site/terms_use) unless CC License in place (see abstract).

ductor Wafer Cleaning Technology, W. Kern, Editor, p. 280, Noyes Publications, Park Ridge, NJ (1993).
25. N. Miki, H. Kikuyama, I. Kawanabe, M. Miyashita, and T. Ohmi, *IEEE Trans. Electron Devices*, **ED-37**, 107 (1990).
26. N. Miki, H. Kikuyama, M. Maeno, J. Murota, and T. Ohmi, *IEDM Proc.*, 730 (1988).
27. W. M. Loh, S. E. Swirhun, T. A. Schreyer, R. M. Swanson, and K. C. Saraswat, *IEEE Trans. Electron Devices*, **ED-34**, 512 (1987).
28. J. Santander, M. Lozano, and C. Cane, *ibid.*, **ED-40**, 944 (1993).
29. C. C. Tang and D. W. Hess, *Appl. Phys. Lett.*, **45**, 633 (1984).
30. J. E. J. Schmitz, M. J. Buiting, and R. C. Ellwanger, in *Tungsten and Other Refractory Metals for VLSI Applications IV*, R. S. Blewer and C. M. McConica, Editors, p. 27 (1988).

Thermal Oxidation of Tungsten-Based Sputtered Coatings

C. Louro and A. Cavaleiro

Departamento de Engenharia Mecânica-Polo II, Pinhal de Marrocos, 3030 Coimbra, Portugal

ABSTRACT

The effect of the addition of nickel, titanium, and nitrogen on the air oxidation behavior of W-based sputtered coatings in the temperature range 600 to 800°C was studied. In some cases these additions significantly improved the oxidation resistance of the tungsten coatings. As reported for bulk tungsten, all the coatings studied were oxidized by layers following a parabolic law. Besides WO_3 and WO_x phases detected in all the oxidized coatings, TiO_2 and $NiWO_4$ were also detected for W-Ti and W-Ni films, respectively. WO_x was present as an inner protective compact layer covered by the porous WO_3 oxide. The best oxidation resistance was found for W-Ti and W-N-Ni coatings which also presented the highest activation energies (E_a = 234 and 218 kJ mol^{-1}, respectively, as opposed to $E_a \approx$ 188 kJ mol^{-1} for the other coatings). These lower oxidation weight gains were attributed to the greater difficulty of the inward diffusion of oxygen ions for W-Ti films, owing to the formation of fine particles of TiO_2, and the formation of the external, more protective layer of $NiWO_4$ for W-N-Ni coatings.

Introduction

Much research work has been carried out in the last few decades on the development of hard coatings for mechanical applications. Besides very high hardness and adhesion, these coatings should be thermally stable and oxidation resistant in order not to fail when service temperatures reach several hundred degrees Celsius. For example, during cutting operations temperatures as high as 900°C can be reached at the tip of the tool.

Hard coatings of the system W-N/C-M (M=Ti, Ni) have been developed as an alternative to titanium-based coatings, which are extensively used in industrial applications. In spite of the very high hardness (in some cases over 45 GPa) and high scratch-test adhesion (critical loads of over 60 N when the coating is deposited on high-speed steel), some of these coatings do not exhibit corresponding excellent behavior in their applications, particularly in cutting operations. The influence of interstitials and of the M elements (as defined) on the mechanical properties of tungsten-based coatings is known; however, in order to understand the cutting performance of these coatings, more knowledge is needed about the influence of these elements on oxidation resistance at high temperatures.

In the development of high-temperature bulk materials, it was observed that oxidation resistance could be improved by the addition of "active elements." Many suggestions have been put forward to explain the effects of these elements. For example, it has been suggested that active elements can act as preferential nucleation sites in the oxidation process, leading to the formation of a protective scale; that active elements can form an intermediate inner oxide layer which acts as a diffusion barrier or as a mechanical buffer; that active elements can reduce the accumulation of voids at the oxide-alloy interface; and that active elements can modify the oxide morphology.[1-3]

The modification of the oxide microstructure and the presence of active elements, either in solid solution, segregated, or as precipitates in the oxide scale, can have an influence on the diffusion rates and the mechanical properties of the oxide scales, playing an important role in the oxidation behavior of the materials.

The beneficial influence of certain reactive elements, such as Al and Cr, on oxidation behavior at high temperatures is a well-known phenomenon,[1,4] but very little is known about the influence of other reactive elements, such as Ti and Ni. Moreover, in spite of the large amount of research work carried out on the high-temperature oxidation behavior of tungsten and tungsten-based alloys, very little is known about its behavior in the form of thin coatings.

In a previous paper[5] we presented the influence of Ti and Ni on the thermal behavior of sputtered W-N coatings in the temperature range 600 to 800°C. It was found that W-N-Ni films presented a much higher oxidation resistance than single W-N and W-Ti-N films. In this paper we present the results of a more global investigation comprising our previous study and extended to sputtered W coatings deposited from single or compound targets (with Ni and Ti) in a nonreactive atmosphere.

Experimental

Deposition

The films were deposited by dc reactive magnetron sputtering with a specific target power density of 10 W cm^{-2} and a negative substrate bias of 70 V. Targets were W, W-10%Ti, and W-10%Ni (mass fractions). When the reactive mode was used the N_2/Ar partial pressure ratio was 1/2, for a total deposition pressure of 3×10^{-3} Pa. The substrates ($5 \times 5 \times 1$ mm) of steel (W1 - AISI) were polished down to a diamond paste of 1 μm. To completely coat the entire surface, the substrates were glued with precision in one of its lateral faces. Owing to the rotational movement of the substrate holder, all the faces were uniformly coated. Before deposition, the sputtering chamber was evacuated by a turbomolecular pump down to a final pressure of 10^{-4} Pa. The substrate surfaces were then ion cleaned by an ion gun. The cleaning procedure included a first electron heating up to temperatures close to 450°C and afterward, Ar^+ bombardment for 8 min (ion gun settings at 20 A, 40 V, substrates at −120 V). The deposition time was selected such that a final thickness in the range 3 to 4 μm

Downloaded on 2014-04-28 to IP 140.113.38.11 address. Redistribution subject to ECS terms of use (see ecsdl.org/site/terms_use) unless CC License in place (see abstract).